Journal of Visualization, Vol. 5, No. 4 (2002) 327-334

Parallel Computation and Numerical Visualization for Non-Uniform Particles Included in Gas and Liquid Flows

Ushijima, S.* and Nezu, I.*

* Department of Global Environment Engineering, Kyoto University, Kyoto-shi 606-8501, Japan.
email: ushijima@gee.kyoto-u.ac.jp

Received 26 February 2002.
Revised 19 April 2002.

***Abstract*:** A parallel computation method has been proposed for the mixing and segregation of granular mixture included in gas and liquid flows. In this method, a three-dimensional (3D) computational volume is decomposed into multiple sub-blocks and their geometries are represented by 3D body-fitted coordinates. The fluid-particle interactions are treated by two types of models: a two-way model for liquid-solid flows and a one-way model in case of gas-solid flows. The computations of the particle motions in the multiple sub-blocks are executed simultaneously on the basis of the distinct element method (DEM). Since a graphic process is also executed as one of the parallel jobs, the particle distributions can be visualized during the computations. The computational method was applied to the gas-solid flows consisting of different diameters and densities in the horizontal and inclined cylinders rotating around their axes. From the comparison with the experimental results, nearly uniform mixing and particle segregation are successfully predicted in the oscillating liquid flows. In addition, it has been indicated that the particle pathline is very effective to visualize and understand the flow patterns of the particles with different properties. The result of the computations for the liquid-solid flows demonstrated that the vertical segregation of the non-uniform particles is reasonably reproduced.

***Keywords*:** parallel computation, multiblock grid, multi-phase flow, particle segregation, particle pathline.

1. Introduction

The accurate estimation for the mixing and segregation process of granular mixture consisting of non-uniform particles is essential in various engineering subjects related to gas-solid and liquid-solid flows. In the present study, a parallel computation method has been developed to predict the Lagrangian behaviors of individual particles with a distinct element method (DEM) (Cundall and Strack, 1979). A multi-block parallel computation technique proposed for CFD (Ushijima et al., 1998) is employed to decrease computational time as well as to deal with the complicated boundary shapes. In this technique, a three-dimensional computational volume is decomposed into multiple sub-blocks and the computations of the particles in the sub-blocks proceed simultaneously exchanging necessary messages concerning the particle movements and contacts among the sub-blocks. The computational efficiency has been confirmed by applying it to the uniform particles in a horizontally rotating cylinder (Ushijima and Nezu, 2000). In particular, in the case of liquid-solid flows, the computations for liquid and solid phases proceed simultaneously, taking account of the interactive effects. In addition, in the present computational method, a graphic process is also included as one of the parallel jobs to visualize the particle distributions during the unsteady computations.

This method has been applied to the gas-solid flows in horizontal and inclined cylinders rotating around

their axes. From the comparison with the experimental results, it has been shown that the nearly uniform mixing and segregation of the different particles are reasonably predicted. It is also indicated that the particle pathlines enable us to understand the flow patterns for the particles with different properties, which are closely related to their mixing and segregation processes. Furthermore, it has been demonstrated that the vertical segregation of non-uniform particles is successfully predicted in an oscillating liquid flow with the present method.

2. Numerical Procedure

2.1 Generation of Coordinates for Sub-blocks

A three-dimensional computational volume is decomposed into multiple sub-blocks with the suitable sections set up by a user. Since the decomposed sub-blocks have more simplified geometry than that of the original computational domain, the boundary shapes of the sub-blocks are accurately represented by generating three-dimensional body-fitted coordinates (3D BFC) (Thompson et al., 1985). The 3D BFC are generated by the iterative calculation of the following equation as done by Ushijima (1994):

$$\left(\frac{\partial^2 x_i}{\partial\xi_p\partial\xi_q}\right)^*\left(\frac{\partial\xi_p}{\partial x_j}\right)^*\left(\frac{\partial\xi_p}{\partial x_j}\right)^* + \frac{\partial^2 x_i}{\partial\xi_r\partial\xi_s}\left(\frac{\partial\xi_r}{\partial x_j}\right)^*\left(\frac{\partial\xi_s}{\partial x_j}\right)^* + P_m\left(\frac{\partial x_i}{\partial\xi_m}\right)^* = 0 \tag{1}$$

where x_i and ξ_m are spatial coordinates in the physical and computational spaces respectively. In Eq. (1), subscripts take $p \neq q$ and $r = s$, and the Einstein summation rule is applied to the terms having same subscripts twice. The control function P_m may be utilized to adjust the mesh intervals in the physical space. The derivatives with asterisks in Eq. (1) are evaluated with cubic spline interpolations to increase the numerical accuracy of the transformation between two spaces (Ushijima, 1994).

2.2 Computations of Liquid Phase

The liquid flows including particles are predicted with Eulerian governing equations by a finite difference method. The governing equations for a liquid phase consist of the ensemble-average continuity and momentum equations, which are derived from a liquid-solid two-fluid model, together with the transport equations for turbulence energy k and its dissipation rate ε. The continuity and momentum equations (Ushijima and Nezu, 2001) are given by

$$\frac{\partial\Phi}{\partial t} + \frac{\partial}{\partial x_i}\left(\Phi U_{fi}\right) = 0 \tag{2}$$

$$\frac{D_f U_{fi}}{Dt} = \frac{1}{\Phi}F_i - \frac{1}{\Phi}\frac{1}{\rho_f}\frac{\partial P}{\partial x_i} - \frac{1}{\Phi}\frac{\partial}{\partial x_j}\left(\Phi\overline{u'_{fi}u'_{fj}}\right) + \nu_f\frac{\partial^2 U_{fi}}{\partial x_j^2} + R_i \tag{3}$$

The instantaneous values are separated into ensemble-average and fluctuating quantities. Thus, the velocity components in the liquid and solid phases, bearing subscripts f and p respectively in this paper, are written as $u_{fi} = U_{fi} + u'_{fi}$ and $u_{pi} = U_{pi} + u'_{pi}$. Similarly, pressure p in the liquid phase and the volumetric concentration of the solid phase c are given by $p = P + p'$ and $c = C + c'$ respectively. In Eqs. (2) and (3), Φ is given by $1 - C$. The interactive force between two phases, R_i in Eq. (3), is calculated as the summation of the forces received by the particles included in a computational grid cell. Thus, it is assumed that the magnitude of the cell-averaged interactive forces are of the order of the Reynolds-averaged ones in this model, which might be improved in further study. The transport equations for k and ε are assumed to be same as those in the single phase flows, assuming that the small scale turbulence is in the isotropic conditions.

The governing equations are discretized in the computational space on a Lagrangian scheme. The convection terms are evaluated using LCSI method (Ushijima, 1994), in which local cubic spline functions are applied to spatial interpolations. It has been confirmed that the accuracy of LCSI method is better than that of third-order upwind difference method (Ushijima, 1994).

2.3 Particle Computation with DEM

The particle motions included in the sub-blocks are solved with distinct element method (DEM). The governing equations of solid particles consist of translational and rotational motions:

$$m\frac{d^2\boldsymbol{x}}{dt^2} = \boldsymbol{F}_G + \boldsymbol{F}_B + \boldsymbol{F}_c \tag{4}$$

$$I\frac{d\boldsymbol{\omega}_p}{dt} = \boldsymbol{T}_G + \boldsymbol{T}_C \tag{5}$$

where m denotes the mass of a particle, I, the moment of inertia, $\boldsymbol{x}$, the position vector and $\boldsymbol{\omega}_p$, the angular velocity vector. The particulate flows dealt within the present study are surrounded by a gas or liquid phase. Thus, the forces, $\boldsymbol{F}_G$, $\boldsymbol{F}_B$ and $\boldsymbol{F}_C$ appearing on the right hand side of Eq. (4) are the fluid-solid interactive force, buoyancy and particle-particle (or particle-wall) contact forces, respectively. The torques, $\boldsymbol{T}_G$ and $\boldsymbol{T}_C$ in Eq. (5), arise from the interaction with a surrounding fluid and from the contact with other particles and boundaries, respectively.

In the DEM, the solid particles and boundaries are treated as elastic bodies rather than rigid ones. This assumption allows us to calculate the interaction of many particles much efficiently, since we need to take account of the contact forces arising from only the particles with which the object is directly in contact. The contact forces acting on a particle are modeled by spring-dashpot mechanism and a friction slider related to the shear force. The normal contact force $\boldsymbol{F}_{Cn}$ is calculated from the spring-dashpot model using the following relationship:

$$\boldsymbol{F}_{cn} = -k_n\boldsymbol{d}_n - \eta_n\boldsymbol{v}_{nr} \tag{6}$$

The first term on the right hand side of Eq. (6) is evaluated by the force-displacement law with normal stiffness k_n and relative displacement vector $\boldsymbol{d}_n$ in the normal direction. The second term is calculated with damping constant η_n and relative normal velocity vector $\boldsymbol{v}_{nr}$.

The evaluation of the shear contact force $\boldsymbol{F}_{Ct}$ depends on whether the particle slides on the contacting surface or not. Firstly, the shear contact force is calculated from the spring-dashpot model.

$$\boldsymbol{F}_{ct} = -k_n\boldsymbol{d}_t - \eta_t\boldsymbol{v}_{tr} \tag{7}$$

where k_t denotes shear stiffness, $\boldsymbol{d}_t$, the relative displacement vector in tangential direction, η_t, the shear damping coefficient and $\boldsymbol{v}_{tr}$, the relative tangential velocity vector. In order to evaluate the relative velocity $\boldsymbol{v}_{tr}$, relative angular velocity is taken into account in addition to the translational velocity in the tangential direction. On the other hand, the friction force is calculated with a Coulomb-type friction model and when the following relationship is satisfied, a slippage occurs on the surface.

$$\left|\boldsymbol{F}_{ct}\right| > \mu_t\left|\boldsymbol{F}_{cn}\right| \tag{8}$$

In this case, the shear contact force equals the friction force given by the right hand side of Eq. (8). Otherwise, no slippage occurs and the shear contact force is calculated by Eq. (7). All contact forces are evaluated with the above procedures and finally they are added up. The obtained normal contact force corresponds to $\boldsymbol{F}_C$ on the right hand side of Eq. (4), while the moment $\boldsymbol{T}_C$ which appears on the right hand side of Eq. (5), is calculated from the derived shear contact force.

In the present multi-block computations, it is necessary to deal with the contact forces acting between two particles included in the different two sub-blocks. This contact usually occurs near the common boundary surface shared by two sub-blocks. To detect such inter-block contacts correctly, near-boundary volumes are set up inside of the shared surfaces in both sub-blocks as shown in Fig. 1. The particle properties, such as the particle position and its diameter, included in the near-boundary volumes are exchanged through a master process between two sub-blocks. Thus, the judgments of inter-block contacts are performed as if the exchanged near-boundary volumes are added on the outside of the shared surfaces. In this way, the continuous evaluation of the particle contacts among multiple sub-blocks can be maintained.

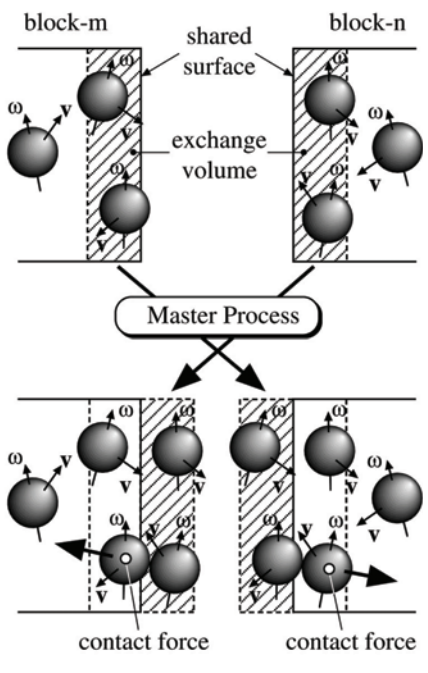

Fig. 1. Detection of inter-block contacts.

3. Application to Particulate Flows

3.1 Experiments of Gas-Solid Flows in Rotating Cylinder

Two components among three types of particles (N3, N6 and A3), as shown in Table 1, were selected and mixed in a cylinder rotating around its axis. The coefficients of restitution e in Table 1 were experimentally obtained. The diameter D and axial length L of the cylinder are 50 mm and 90 mm, respectively. The rotational speed is about 0.93 revolutions per second. As indicated in the experimental conditions in Table 2, the angle θ between its axis and horizontal surface is zero (horizontal) and 6.1 degrees (inclined).

Table 1. Particles used in experiments.

Particles	Material	d (mm)	ρ_p (g/cm^3)	e
N3	nylon	3.3	1.14	0.77
N6	nylon	6.4	1.14	0.78
A3	almina	3.3	3.60	0.82

Table 2. Experimental conditions (inclined angle and number or particles).

Case	θ (deg)	N3	N6	A3
H-N3A3	0.0	150	0	150
H-N6A3	0.0	0	50	150
I-N3A3	6.1	150	0	150
I-N6A3	6.1	0	50	150

In the experiments, the selected particles were uniformly mixed and flatly settled in the cylinder to form the suitable initial conditions. During the rotation, the particle distributions were recorded from above by a video camera.

Figure 2 shows the experimental results analyzed from the video images, which indicate the typical distributions in each case. When $\theta = 0$, N3 and A3 particles are almost uniformly mixed as shown in Fig. 2 (a), while N6 and A3 particles are clearly separated as indicated in Fig. 2 (b). In H-N6A3, A3 particles gather on the rising side wall, while relatively fewer N6 particles remain behind of them and they are dominantly distributed near the both ends of the cylinder. Wightman and Muzzio (1998) reported the similar experimental results, in which the particles with larger diameter tend to gather both ends of a rotating drum.

In the inclined rotating cylinder, in contrast to H-N3A3, N3 and A3 particles are separated as shown in Fig. 2 (c). The higher density A3 particles gather at the higher side of the inclined cylinder. Similar results are obtained in I-N6A3 indicated in Fig. 2 (d), which is clearly different from H-N6A3.

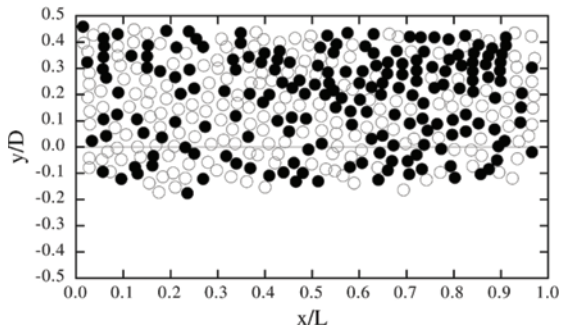

(a) H-N3A3

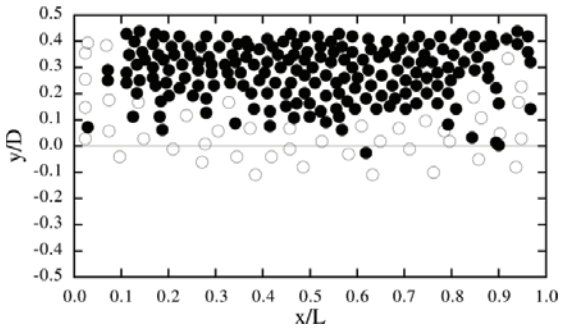

(b) H-N6A3

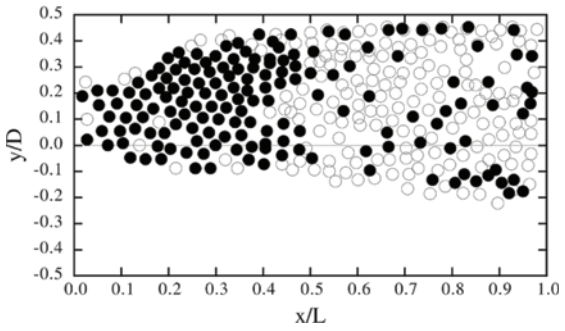

(c) I-N3A3 (Left is higher than right)

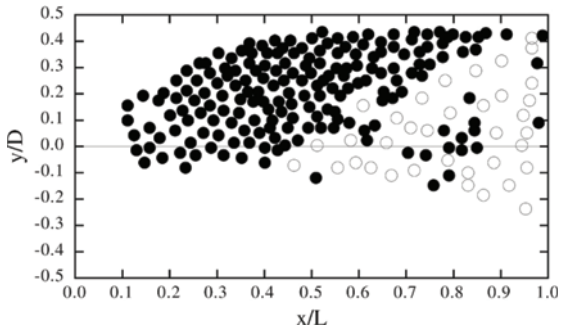

(d) I-N6A3 (Left is higher than right)

Fig. 2. Experimental results (● = A3, ○ = N6 or N3).

3.2 Predicted Results and Particle Distributions

The present computational method has been applied to all cases in Table 2 with 4-block decomposition. The time increment Δt is 1.0×10^{-5} sec and Young's modulus, Poisson's ratio and coefficient of friction are set at 5.0×10^{4} (N/m), 0.46 and 0.4 for all particles and boundaries. Most of these parameters were determined through the experiments. The graphic process was executed every 100 steps of particle calculation, which brought about no computational load on the particle computations.

The typical particle distributions obtained by the graphic process are shown in Fig. 3. Since the continuous snapshots are saved by the graphic process, dynamic movements of the particles are actually visualized in a movie style. The particle distributions in Fig. 3 indicate the same tendencies as observed in experiments; nearly uniform mixing in H-N3A3 and particle segregation arising in the other cases.

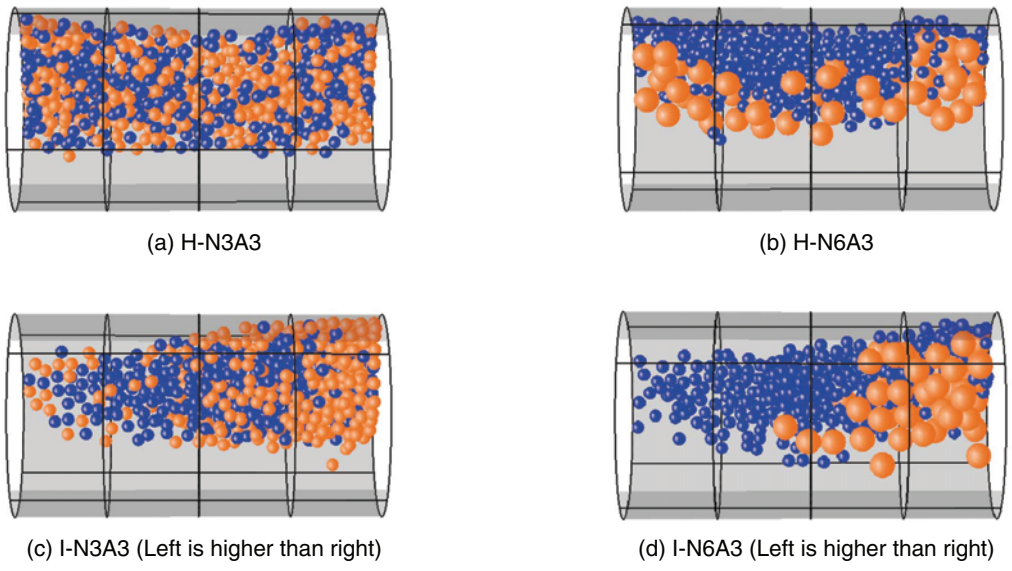

Fig. 3. Computed results (blue [black] = A3, red [gray] = N3 or N6).

3.3 Numerical Visualization with Particle Pathlines

In experiments, it is generally difficult to visualize the inside flow patterns arising in particulate flows, since particles are usually opaque and difficult to track individual particle movements. Thus, such measurements have been conducted by observing particle distributions only in the surface regions and taking samples at some limited positions. On the contrary, the 'numerical experiments' as done by the present study enables us to capture the velocity components and positions in 3D space, which can be utilized to understand the mixing and segregation processes in the non-uniform particulate flows.

Particle pathlines, drawn for each components included in the non-uniform particles, are very effective to capture the flow pattern indicated by different particles. The particle pathlines are obtained as the trace lines for the time- and cell-averaged particle velocities, which correspond to the pathlines in the usual flow-visualization. Figure 4 shows the derived pathlines for all cases. In H-N3A3, as shown in Fig. 4 (a), the pathlines for N3 and A3 show the similar patterns, which results in the uniform mixing as confirmed in the experiments. In H-N6A3, on the other

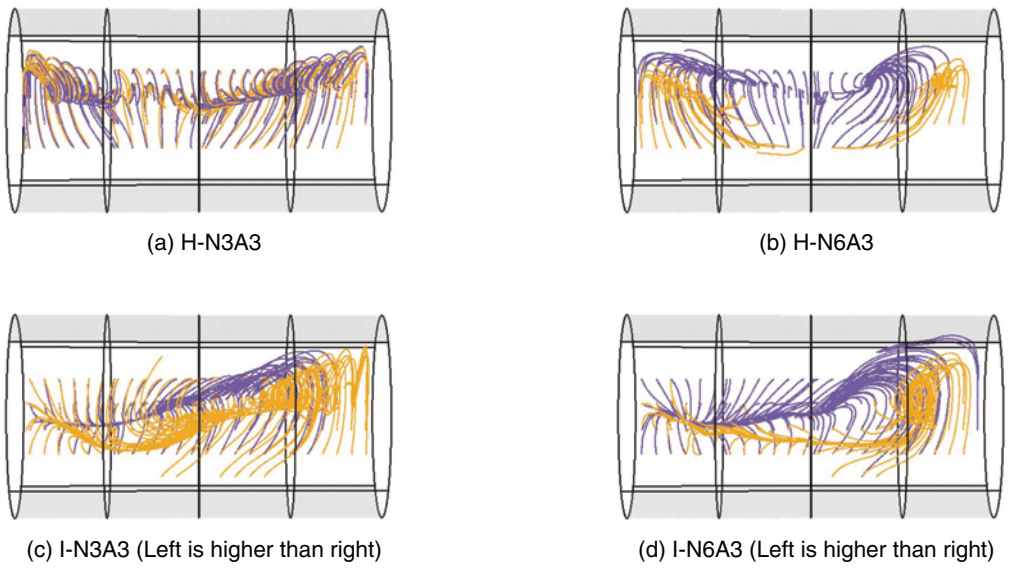

Fig. 4. Particle flow patterns visualized by particle pathlines (violet [black] = A3, orange [gray] = N3 or N6).

hand, the pathlines of N6 extend to both ends in the cylinder, corresponding to the gathering of N6 in the area. It is noted that the independent 'particle vortex tubes' for N3 and A3 are visualized in I-N3A3 in Fig. 4 (c). Since the same tendency is found in I-N6A3, it is suggested that the two types of particles take independent flow patterns due to the particle forces arising between the contact surface of their pathlines.

3.4 Granular Mixture in Oscillating Liquid Flows

The proposed computational method was applied to granular binary mixture included in an oscillating liquid flow in a horizontal pipe. The diameter and axial length of the pipe are 50 mm and 90 mm respectively. The oscillating flow was created by controlling the pressure boundary conditions on both ends, while periodic boundary conditions were applied to the fluid velocity and particle movements. The non-uniform particles consist of two components; S-particle and L-particle. The diameter and specific gravity of the S-particle are 2 mm and 2.0 respectively, while those of the L-particle are 3 mm and 2.0. The number of S- and L-particles are 1,067 and 533 in the computational volume.

In the initial condition, the granular mixture is randomly accumulated in a horizontal pipe in a static flow field as shown in Fig. 5 (a). The computational volume was separated into four sub-blocks as shown in Fig. 5 (a). The computations for liquid and solid phases in each sub-block are assigned to one PC. Thus four PCs were used to calculate both phases in four sub-domains, while another PC was applied to the graphic process.

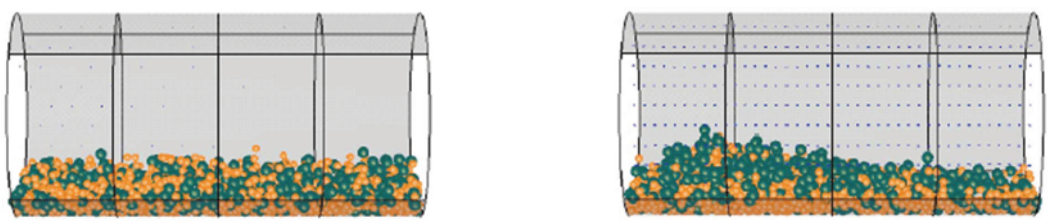

(a) Initial particle distribution (t / T = 0)

(b) Distribution of particles (t / T = 3.15)

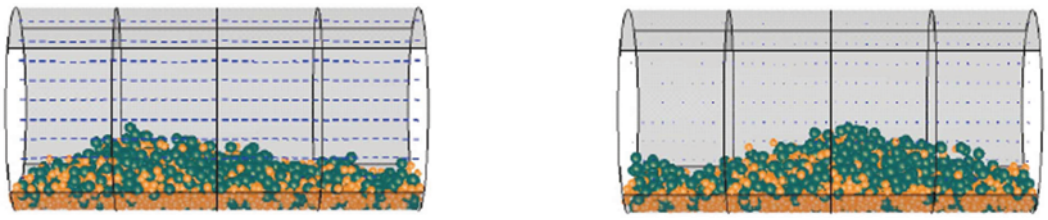

(c) Distribution of particles (t / T = 3.33)

(d) Distribution of particles (t / T = 3.51)

Fig. 5. Predicted particle distributions in liquid flows (green = L-particles, orange = S-particles).

In the present numerical experiment, pressure gradient was given to the initial condition to make the liquid phase flow in an axial direction. The pressure gradient between both ends is altered when the axial velocity component at the center of the pipe has reached 1.5 m/s. The solid particle leaving from one end enters again on the other end having the same velocity and same position on the circular section.

The results of the unsteady computation are shown in Figs. 5 (b)-(d). The L-particles with a larger diameter are localized near the surface region of the accumulated particles as shown in Figs. 5 (b)-(d). In addition, the height of the accumulated particles, which was nearly flat in the initial condition as shown in Fig. 5 (a), gradually deformed in the axial direction like sand waves. The predicted particle segregation agrees well with the tendency generally observed in granular mixture in liquid flows.

4. Concluding Remarks

A multi-block parallel computational method has been proposed to predict Lagrangian behaviors of particulate flows on the basis of DEM. A 3D computational volume is decomposed into multiple subdomains and the computations of particles proceed simultaneously. Therefore, this computational technique allows us to deal with a

fairly complicated-shaped 3D computational domain as well as to increase the computational efficiency, in other words, to deal with much more number of particles than usual.

The developed computational method was applied to the gas-solid flows confined in a rotating cylinder. The axis of the cylinder is set at horizontal and inclined by 6.1 degrees from the horizontal surface. From the comparison with the experimental results, it has been shown that the uniform mixing and clear segregation are successfully predicted with the present method. In addition, it has also been demonstrated that the particle pathlines, drawn for each components in the non-uniform particles, are very effective to capture their flow patterns and available to understand their mixing and segregation processes.

In case of the liquid-solid flows, the fluid-particle interaction is taken into account in the unsteady computation through the message passing in parallel numerical procedures. As a result of the numerical experiment for liquid-solid flows, it was shown that the vertical segregation of the non-uniform particles is successfully predicted in an oscillating turbulent flow with the present method.

References

Cundall, P. A. and Strack ,O. D. L., A Discrete Numerical Model for Granular Assemblies, Geotechnique, 29-1 (1979), 47-65.

Thompson, J. F., Warsi, Z. U. A. and Mastin ,C. W., Numerical Grid Generation, (1985), Elsevier Science, New York.

Ushijima, S., Prediction of Thermal Stratification in a Curved Duct with 3D Boundary-fitted Co-ordinates, International Journal for Numerical Methods in Fluids, 19 (1994), 647-665.

Ushijima, S. and Nezu, I., Numerical Visualization of Granular Mixture in a Rotating Cylinder, 9th Int. Symp. on Flow Visualization, (2000), 400-1-10.

Ushijima, S. and Nezu, I., Numerical Prediction of Liquid-solid Turbulent Flows on Moving Boundaries with ALE Method, Turbulence and Shear Flow Phenomena, 2 I (2001), 283-288.

Ushijima, S., Yoneyama, N. and Tanaka, N., Multiblock-parallel Computations of 3D Flows in Complicated-shaped Hydraulics Structures, Proc. 7th Int. Symp. on Flow Modeling and Turbulence Measurements, (1998), 347-354.

Wightman, C. and Muzzio, F. J., Mixing of Granular Material in a Drum Mixer Undergoing Rotational and Rocking Motions, II. Segregating Particles, Powder Technology, 98 (1998), 125-134.

Author Profile

Satoru Ushijima : He received master's degree in civil engineering in 1984 and his doctor's degree in 1990 from Kyoto University. He worked in Central Research Institute of Electric Power Industry (CRIEPI) from 1984 to April, 2000. Since April 2000, he has been working in the department of Global Environment Engineering in Kyoto University and his current position is an associate professor. His recent researches are related to the development and application of CFD techniques to multiphase and other complicated flows.

Iehisa Nezu: He received his B.E. (1971), M.E. (1973) and D.E. (Ph.D.) (1977) degrees from Kyoto University under the supervision of Prof. H. Nakagawa. He stayed in Karlsruhe University in 1983 and collaborated with Prof. W. Rodi. He was awarded as “Thesis Prize” JSCE (1976), “Karl Emil Hilgard Hydraulic Prize” by ASCE (1987) and “The Most Splendid Paper APD-IAHR Award” by IAHR (1998). His IAHR Monograph entitled “Turbulence in Open-Channel Flows”, Balkema Pub. (1993) is well known in hydraulic community. He is a full professor and director of Hydraulics Laboratory in Kyoto University since 1996.